Volume 55 | Number 84 | 28 October 2019 | Pages 12583–12724

ChemComm

Chemical Communications

rsc.li/chemcomm

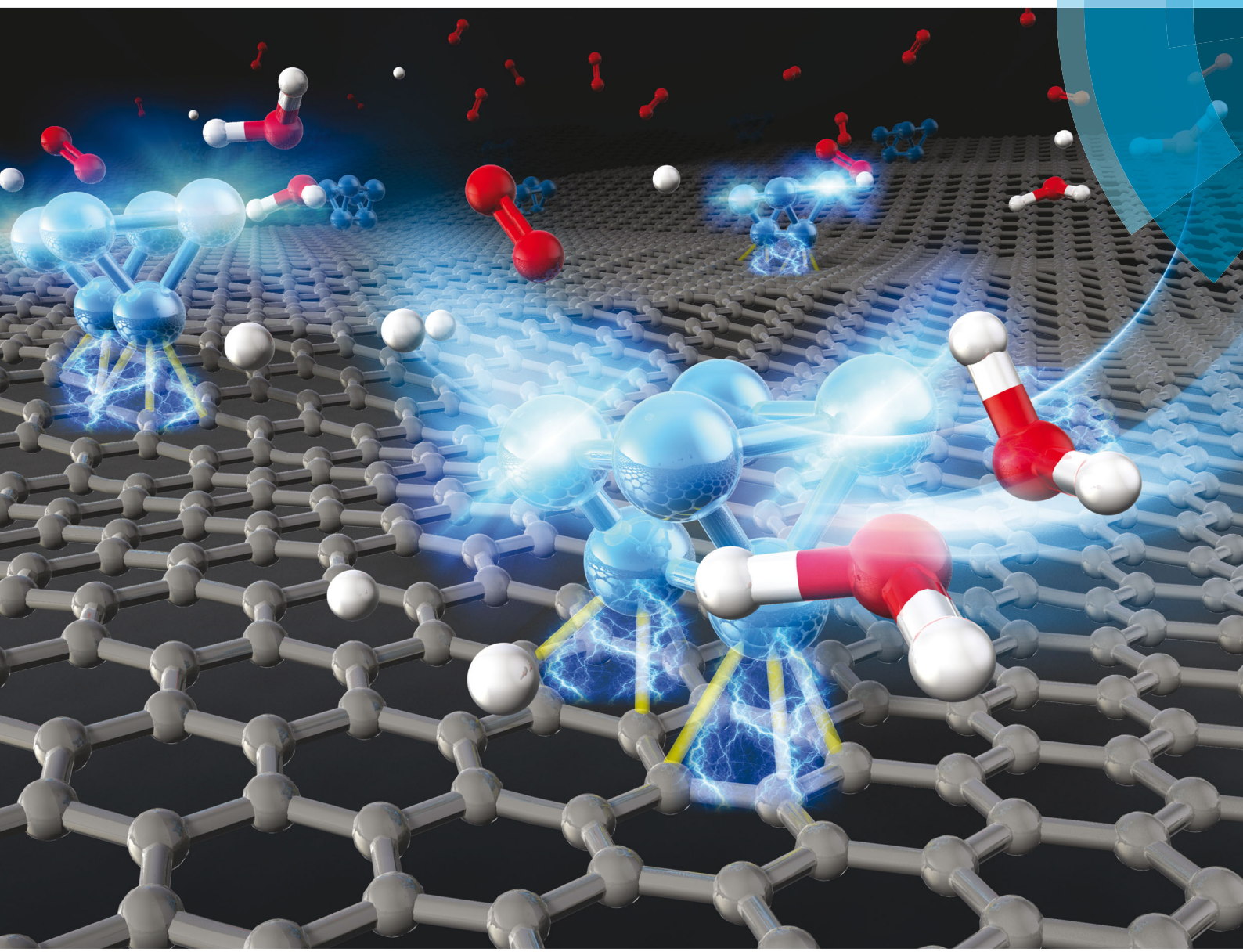

ISSN 1359-7345

ROYAL SOCIETY OF CHEMISTRY | Celebrating IYPT 2019

COMMUNICATION

H. Tsunoyama, A. Ohnuma *et al.*

Enhanced oxygen reduction activity of platinum subnanocluster catalysts through charge redistribution

ChemComm

COMMUNICATION

View Article Online
View Journal | View Issue

Cite this: *Chem. Commun.*, 2019, **55**, 12603

Received 15th August 2019,
Accepted 17th September 2019

DOI: 10.1039/c9cc06327g

rsc.li/chemcomm

Enhanced oxygen reduction activity of platinum subnanocluster catalysts through charge redistribution†

Hironori Tsunoyama, ‡[a] Akira Ohnuma, ‡[b] Koki Takahashi,[a] Archana Velloth,[c] Masahiro Ehara, [c] Nobuyuki Ichikuni, [d] Masao Tabuchi[e] and Atsushi Nakajima *[a]

Single-size platinum Pt_6 subnanoclusters exhibit superior mass-specific and surface-specific activities for the oxygen reduction reaction. The enhanced activity is attributed to polarized electron distributions based on rigorous structure characterization by X-ray absorption fine structure spectroscopy and density functional theory.

The development of durable and active catalysts with high atomic efficiency has been a key issue for a sustainable world, where size-selected, sub-nanoscale clusters (sub-NCs) consisting of a few to tens of atoms have been strong potential candidates attributable to their high surface area and tunability of activity by "atomicity". A wide variety of catalytic properties of sub-NCs have been extensively reported,[1–8] and among the various uses for the catalytic transformations, fuel cell (FC) technology appears to be a promising way to reduce environmental loads based on the potential of a principally carbon-free energy source.[9–11] Among the various types of FCs, proton-exchange membrane FCs have attracted much attention due to their low-temperature operation, which makes them particularly suitable for mobile vehicles. Although various technological advancements are needed to upgrade FCs, the development of more active catalysts is required for the cost reduction and the downsizing of FC units. Since the activity for the cathodic reaction, the oxygen reduction reaction (ORR), is lower than that for the anodic hydrogen oxidation reaction, improvements in mass specific activity (MA/A g_{Pt}^{-1}) for the ORR are essential. To this end, various active catalysts have been developed so far, using *e.g.*, core–shell, alloy, and unique nanostructures,[9,10,12–14] by tuning the reactivity through ligand, strain, and ensemble effects.[15,16]

For platinum (Pt)-based nanoparticle (NP) catalysts, one of the convincing arguments for catalyst development is to increase the surface-to-volume ratio through downsizing the catalytic NPs; MA increases with the surface ratio, and reaches a constant value above 80 m^2 g_{Pt}^{-1}.[14] In terms of high surface ratio, NCs with less than ten atoms are good candidates to enhance the activity. Although the atomicity is a unique parameter for the activity in monometallic Pt NCs, size specificity is still controversial;[2,17–24] the difficulty arises from the complex nature of catalysts, *e.g.*, non-systematic variation of structures with the size and effect of surrounding materials (supports and ligated molecules). For a systematic understanding of NC catalysis, a dry fabrication method which reduces the complexity through the entirely clean nature of the synthetic procedure carried out under high vacuum conditions, facilitates the catalysis preparation of naked NCs;[2,3,25–30] high surface specific activity (SA) of Pt_{46} NCs has been reported at high coverage.[2] Despite numerous efforts, the correlation between activity and structure has not been elucidated so far, which is crucial to establish a reliable guiding principle for NC catalysts.

We have demonstrated herein that the ORR activity of Pt_6 sub-NCs supported on a glassy carbon (GC) electrode shows superior activity compared to a standard Pt/C catalyst, the origin of which is discussed in terms of the geometric and electronic structures investigated *via* X-ray absorption fine structure (XAFS) spectroscopy and density functional theory (DFT) calculations.

Pt NC catalysts were prepared by soft-landing of size-selected NCs using a high-flux single-size NC generation system, nanojima®-NAP01,[31,32] combined with a quadrupole mass filter (Fig. S2, ESI†), where the collision energy of the NCs was kept under 1 eV per atom to avoid fragmentation during the deposition. In order to suppress agglomerations of NCs on the GC surface,

[a] *Department of Chemistry, Faculty of Science and Technology, Keio University, 3-14-1 Hiyoshi, Kohoku-ku, Yokohama, Kanagawa 223-8522, Japan. E-mail: nakajima@chem.keio.ac.jp*
[b] *New Field Pioneering Division, Toyota Boshoku Corp., 1-1 Toyoda-cho, Kariya, Aichi 448-8651, Japan*
[c] *Department of Theoretical and Computational Molecular Science, Institute for Molecular Science, Myodaiji, Okazaki 444-8585, Japan*
[d] *Department of Applied Chemistry and Biotechnology, Graduate School of Engineering, Chiba University, 1-33 Yayoi-cho, Inage-ku, Chiba 263-8522, Japan*
[e] *Synchrotron Radiation Research Center, Nagoya University, Furo-cho, Chikusa, Nagoya 464-8603, Japan*

† Electronic supplementary information (ESI) available: Mass spectrum of Pt NC, STEM image, XANES spectra, EXAFS fitting results, optimized structures of free and adsorbed Pt NC by DFT calculations, and simulations for XAFS. See DOI: 10.1039/c9cc06327g

‡ Equal contribution.

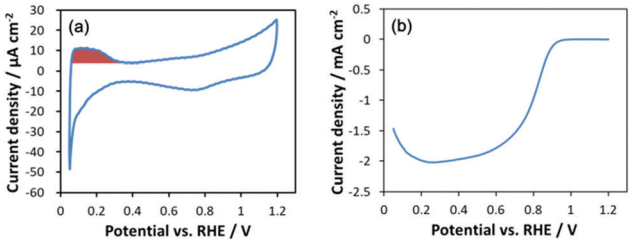

Fig. 1 A cyclic voltammogram under argon (a) and a hydrodynamic voltammogram under oxygen (b) for Pt_6/GC. The red area in (a) corresponds to the desorption of hydrogen. Experimental conditions: concentration of $HClO_4$; 0.1 M and sweep rate; 50 mV s^{-1}.

the density of deposited Pt_6 sub-NCs was kept under 0.5 ML equivalents based on the density of a Pt(111) surface by assuming that the GC electrode has a flat surface. In addition, prepared catalysts were kept under an oxygen-free argon atmosphere until just before the electrochemical (EC) measurements to avoid oxidation of tiny NCs and contamination by organic substances. Successful immobilization of Pt NCs was confirmed by high-resolution scanning transmission electron microscopy as shown in Fig. S3 (ESI†).

Fig. 1a shows a representative cyclic voltammogram under an argon atmosphere. Current for underpotential adsorption/desorption of hydrogen is clearly observed around 0.05–0.3 V_{RHE}. The electrochemically active surface area (ECSA) was evaluated based on the reported procedure[33] by integrating the hydrogen desorption current using a factor of 210 μC cm_{Pt}^{-2}. Surprisingly the ECSA for Pt_6 (Table 1) is *ca.* 0.8 times that of a commercial standard Pt/C catalyst (TEC10E50E, TKK) with a crystallite size of 3 nm, which is a large deviation from the hypothetical surface ratio for such tiny Pt_6 sub-NCs. The origin of the decrease in the ECSA is discussed based on its structure in a later section. A hydrodynamic voltammogram under oxygen (Fig. 1b) represents clear ORR activity despite the ultra-low loading of NC catalysts using the reported procedure.[34] Since high sensitivity measurements for the present ultra-low loading catalyst are susceptible to impurities, it is difficult to evaluate kinetic limiting current density (J_{kin}) from the Koutecky–Levich plot, and so the ORR J_{kin} has been estimated using the Koutecky–Levich equation based procedure reported by Yamamoto and co-workers.[17,18] Despite the relatively lower ECSA for Pt_6, the MA at 0.9 V_{RHE} for Pt_6/GC is 74% higher than that of the standard Pt/C catalyst. Furthermore, the Pt_6 SA at 0.9 V_{RHE} is 2.3 times higher than that for the Pt/C catalyst. For the typical Pt NP catalyst with a diameter larger than 3 nm, the MA increases with increasing ECSA, while SA increases with decreasing ECSA for larger NPs.[14] In this system, both the MA and SA of Pt_6 are higher than those for Pt NPs, which is in sharp contrast to conventional NP catalysts.

Table 1 Catalytic properties for Pt_6/GC[a]

	ECSA[b] (m^2 g_{Pt}^{-1})	MA[c] (A mg_{Pt}^{-1})	SA[d] (mA cm_{Pt}^{-2})
Pt_6/GC	54 (8)	0.52 (8)	0.96 (7)
Pt/C[e]	71 (2)	0.30 (0)	0.42 (1)

[a] Uncertainties are given in parentheses, referred to the corresponding last digit. [b] Evaluated from desorption current of hydrogen. [c] Obtained from kinetic limiting current at 0.9 V_{RHE}. [d] Obtained from kinetic limiting current at 0.9 V_{RHE} and ECSA. [e] Standard Pt/C catalyst (TEC10E50E).

We now discuss the origin of the superior activity of Pt_6/GC catalysts in terms of their geometric and electronic structures through rigorous characterizations using extended XAFS (EXAFS) and DFT calculations. The charge state for deposited Pt_6 sub-NCs is almost neutral based on analysis of the X-ray absorption near edge structure (XANES) as shown in Fig. 2a, where the white-line for the Pt L_3 edge is almost identical with that for bulk Pt foil. Surprisingly the Pt_6/GC catalyst is robust against oxidation under ambient conditions (Fig. S4, ESI†), suggesting that the structure of Pt_6 sub-NCs remains unchanged in EC experiments under an oxygen atmosphere from the EXAFS measurements under argon. The XAFS $\chi(R)$ profile (Fig. 2b) clearly exhibits a radial distribution peak for Pt–Pt bonds; Pt–Pt bond distance and its coordination number (CN) for Pt_6/GC are slightly smaller and much smaller than those for the bulk Pt, respectively (Table S2, ESI†). In order to characterize the Pt_6 structure in detail, we have compared between (1) experimental $\chi(k)$ spectra ($\chi_{obs}(k)$) extracted with the Athena program[35] and (2) those simulated for the calculated equilibrium geometries by the FEFF code[36] ($\chi_{sim}(k)$). As a result of DFT calculations using the VASP program,[37,38] where the GC surface was modeled with a graphene (Gr) structure, seven isomers were found for Pt_6/Gr (Fig. S5, ESI†) within a total energy difference of 0.5 eV. Details of geometry optimization are explained in the ESI.† Based on the matching of the phases between $\chi_{obs}(k)$ and $\chi_{sim}(k)$ spectra for Pt_6/GC, we can safely exclude planar isomers (Pt_6-**1**–**3**) due to the deviation at the higher k regime ($k > 6$ Å^{-1}) (Fig. S6, ESI†). Bent triangular isomers (Pt_6-**4**–**6**) can also be excluded due to a slight phase deviation at $k > 8$ Å^{-1}. By considering the structure scaling (−2% to +2%) for the

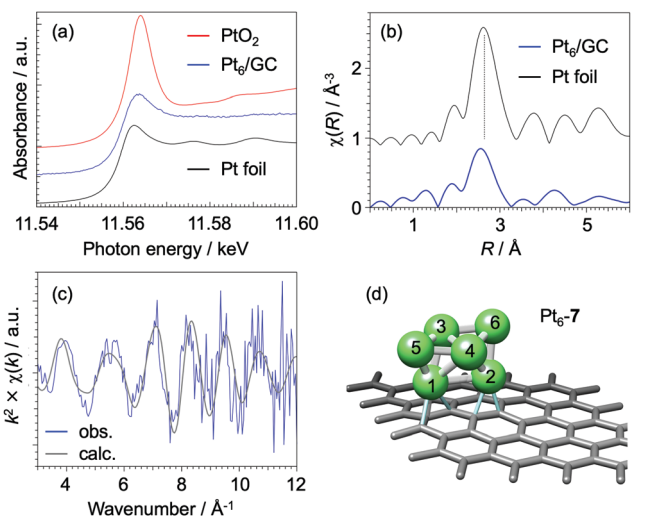

Fig. 2 Results of EXAFS spectroscopy for Pt_6/GC. (a) XANES spectra that have been offset vertically for clarity of presentation, (b) $\chi(R)$ profile obtained by Fourier transform of $\chi(k)$ spectra in the range k = 5–12 Å^{-1}, and (c) observed $\chi(k)$ spectra along with simulation for the most probable isomer of Pt_6-**7**. Simulation conditions: energy shift: +5.0 eV, distance shift: +0.075 Å, Debye–Waller factor: 0.008. (d) Optimized structure for Pt_6-**7** on graphene from DFT calculations.

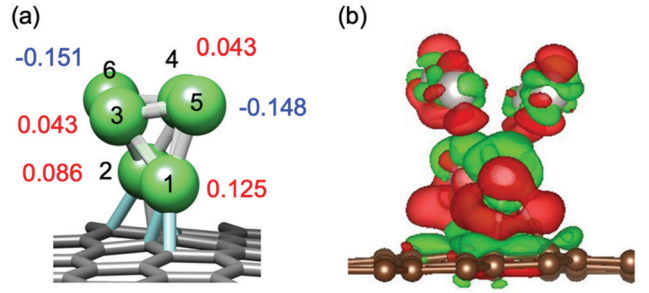

Fig. 3 Atomic charge distribution of Pt_6/Gr (isomer **7**). (a) Bader charge and (b) electron density difference iso-surface; charge depletion and accumulation regions are shown in red and green, respectively.

optimized Pt_6/Gr geometry, the above conclusion is thoroughly supported (Fig. S7, ESI†). Since both the phase and amplitude are quantitatively matched in Fig. 2c, the most probable structure for Pt_6/GC is concluded to be the isomer Pt_6-7 (Fig. 2d). Although the isomer Pt_6-7 is not the most stable one in the DFT calculations, the discrepancy may be explained by the occurrence of a different structure on the GC surface[39] from that on Gr.

The origin of the size-specific activity is discussed in terms of their electronic structure and the reported reaction mechanism for the ORR.[40,41] A Bader charge analysis (Fig. 3a) shows that Pt_6 sub-NC is polarized on the Gr surface; two Pt sites with a low CN (CN = 3, Pt(6) and Pt(5)) are negatively charged (q = −0.15) while the other Pt atoms are positively charged; two Pt not coordinated to Gr (q = +0.04) and two Pt coordinated to Gr (q = +0.09, +0.13). Charge redistribution upon adsorption can be also identified from the electron-density-difference isosurface shown in Fig. 3b; charge accumulation regions are spread over the Pt(5) atom and Pt(1)–Pt(5) bond. In the ORR mechanism,[40,41] dissociative adsorption of molecular O_2 on a Pt site is an important step to $4e^-$ reduction for direct formation of water, which results in higher ORR activity rather than $2e^-$ reduction to form hydrogen peroxide through molecular O_2 adsorption. Electron density tends to accumulate at the apex site in NCs and the negatively charged site is reactive.[42] In a kinetic picture, the first electron transfer step to an O_2 molecule is an important step, where cleaving the O–O bond forms adsorbed atomic oxygen (O*), although the rate determining step for the $4e^-$ reduction pathway in a thermodynamic picture is reduction of adsorbed hydroxy radical species (OH*).[40] To activate the adsorbed molecular O_2 through electron transfer, the d-band center level for a Pt adsorption site plays a crucial role, because a relatively higher d-band-center with respect to bulk Pt(111) enhances the activity.[41] In fact, the d-band-center closely correlates with a partial charge on the site; a partial negative charge pushes the d-band-center up.

Two possibilities can be considered as the reasons for the high activity of Pt_6/GC; (i) the high surface area of Pt_6 and (ii) the site-specific activation of oxygen molecules as described above. The ratio of surface atoms (P_{surf}) in NPs depends on the diameter; P_{surf} values are 45% for Pt_{561} (d = 2.97 nm) and 63% for Pt_{147} (d = 1.89 nm) based on a spherical geometry of cuboctahedron or icosahedron. On the other hand, the Pt_6-7 sub-NC has four outermost Pt atoms and two Pt atoms ligating to carbon, producing a P_{surf} of 66%, which is almost comparable or at most 20% higher than that of the standard Pt/C catalyst (d = 3 nm). Therefore, the effect of surface atom exposure probably plays a minor role in the enhanced activity. In the electronic structure of larger NPs, such as Pt_{309} (d = 2.43 nm), the density of states and d-band-center energy look similar to those for a bulk Pt surface based on DFT.[43] In addition, atomic charge distribution in Pt_{309} NC seems less polarized even after adsorption on Gr, excluding the peripheral atoms.[43] As a result, the ORR activity of NPs is mainly influenced by P_{surf} values as summarized in the previous literature,[14] which has been believed to be a key principle in the catalyst development. On the other hand, Pt_6 is highly polarized (−0.15 to +0.13 e) after adsorption on the Gr (Fig. 3a). As a result of charge redistribution in Pt_6, the average of the d-orbital energy, corresponding to the d-band-center in the bulk, for negatively charged Pt sites is −1.47 eV from the Fermi energy (ε_F), which is higher in energy than other Pt sites (−1.81 to −1.66 eV). The d-orbital-center energy is much higher than the d-band center for larger NPs and the bulk (111) surface.[44] Based on our knowledge of the correlation between the d-band-center and ORR activity,[41] the enhanced MA for Pt_6/GC can be attributed to its electronic structure changed by a large degree of charge separation in the tiny NCs. On the other hand, ECSA determined from hydrogen adsorption/desorption is smaller than the larger NP of Pt/C. This probably originates from site specific adsorption[44] of hydrogen on the smaller NCs, which also supports the idea of a large change in the surface chemical nature for Pt_6 catalysts; Pt sites charged neutral presumably act as adsorption sites for hydrogen. The nature of site-specificity for sub-NCs, originating from a greater flexibility of charge redistribution, will enable much higher activity by further alloying and strong support interactions through electronic interaction (ligand and strain effects)[16] in addition to the geometric ensemble effect.[15]

In conclusion, we have demonstrated superior mass-specific and surface-specific activities of Pt_6 subnanoclusters for oxygen electroreduction, which are 1.7 and 2.3 times higher than the conventional standard Pt/C catalysts with a crystallite diameter of 3 nm. Based on rigorous structure analyses by X-ray absorption fine structure spectroscopy and density functional theory calculations, we have identified the geometric structure of Pt_6. The origin of simultaneous enhancements of SA and MA for ORR, which is unusual in pure metallic Pt catalysts, is attributed to larger charge redistribution in the tiny sub-NC, leading to pushing the d-band-center energy up compared to the NP catalysts. The present study provides an important guideline for catalyst developments and opens "precise NC catalysis chemistry" for a future FC technology.

The authors thank Dr Tomoyuki Nagai for the advice on electrochemical measurements, Dr Kouta Iwasaki for discussion and comments on the manuscript, Mr Motoki Kondo for the experimental support, and Prof. Dr Hidehiro Yasuda and Prof. Dr Kazuhisa Sato for STEM measurements. Development on nanojima® apparatus was supported by Ayabo Corp. The computations were partly performed using Research Center for

Computational Science, Okazaki, Japan. HAADF-STEM measurements were supported by "Advanced Characterization Nanotechnology Platform, Nanotechnology Platform Program of the Ministry of Education, Culture, Sports, Science and Technology (MEXT), Japan" at the Research Center for Ultra-High Voltage Electron Microscopy (Nanotechnology Open Facilities) in Osaka University. This work is partly supported by JSPS KAKENHI of Grants-in-Aid for Scientific Research (A) Grant No. 15H02002 and 19H00890, of Challenging Research (Pioneering) Grant No. 17H06226, and of Grant-in-Aid for Young Scientists (A) Grant No. 15H05475.

Conflicts of interest

The authors declare the following competing financial interest(s): H. T. and A. N. are inventors on JAPAN patent JP 5493139, submitted by JST agency and Ayabo Corp., which covers the nanocluster generator.

Notes and references

1 B. Yoon, H. Häkkinen, U. Landman, A. S. Wörz, J.-M. Antonietti, S. Abbet, K. Judai and U. Heiz, *Science*, 2005, **307**, 403–407.
2 M. Nesselberger, M. Roefzaad, R. F. Hamou, P. U. Biedermann, F. F. Schweinberger, S. Kunz, K. Schloegl, G. K. H. Wiberg, S. Ashton, U. Heiz, K. J. J. Mayrhofer and M. Arenz, *Nat. Mater.*, 2013, **12**, 919–924.
3 A. von Weber and S. L. Anderson, *Acc. Chem. Res.*, 2016, **49**, 2632–2639.
4 S. Yamazoe, K. Koyasu and T. Tsukuda, *Acc. Chem. Res.*, 2014, **47**, 816–824.
5 K. Yamamoto and T. Imaoka, *Acc. Chem. Res.*, 2014, **47**, 1127–1136.
6 R. M. Anderson, D. F. Yancey, L. Zhang, S. T. Chill, G. Henkelman and R. M. Crooks, *Acc. Chem. Res.*, 2015, **48**, 1351–1357.
7 R. Jin, C. Zeng, M. Zhou and Y. Chen, *Chem. Rev.*, 2016, **116**, 10346–10413.
8 Y. Du, H. Sheng, D. Astruc and M. Zhu, *Chem. Rev.*, 2019, DOI: 10.1021/acs.chemrev.8b00726.
9 D. Banham and S. Ye, *ACS Energy Lett.*, 2017, **2**, 629–638.
10 A. Kongkanand and M. F. Mathias, *J. Phys. Chem. Lett.*, 2016, **7**, 1127–1137.
11 B. C. H. Steele and A. Heinzel, *Nature*, 2001, **414**, 345–352.
12 M. K. Debe, *Nature*, 2012, **486**, 43–51.
13 X. Wang, A. Ruditskiy and Y. Xia, *Natl. Sci. Rev.*, 2016, **3**, 520–533.
14 D. Thompsett, in *Handbook of Fuel Cells: Fundamentals, Technology, and Applications*, ed. W. Vielstich, A. Lamm and H. A. Gasteiger, Wiley, Chichester England, 2003, ch. 37, vol. 3, pp. 467–480.
15 H. Li, K. Shin and G. Henkelman, *J. Chem. Phys.*, 2018, **149**, 174705.
16 L. Zhang and G. Henkelman, *J. Phys. Chem. C*, 2012, **116**, 20860–20865.
17 T. Imaoka, H. Kitazawa, W.-J. Chun and K. Yamamoto, *Angew. Chem., Int. Ed.*, 2015, **54**, 9810–9815.
18 K. Yamamoto, T. Imaoka, W.-J. Chun, O. Enoki, H. Katoh, M. Takenaga and A. Sonoi, *Nat. Chem.*, 2009, **1**, 397–402.
19 M. Nesselberger, S. Ashton, J. C. Meier, I. Katsounaros, K. J. J. Mayrhofer and M. Arenz, *J. Am. Chem. Soc.*, 2011, **133**, 17428–17433.
20 M. Rück, A. Bandarenka, F. Calle-Vallejo and A. Gagliardi, *J. Phys. Chem. Lett.*, 2018, **9**, 4463–4468.
21 M. Shao, A. Peles and K. Shoemaker, *Nano Lett.*, 2011, **11**, 3714–3719.
22 F. J. Perez-Alonso, D. N. McCarthy, A. Nierhoff, P. Hernandez-Fernandez, C. Strebel, I. E. L. Stephens, J. H. Nielsen and I. Chorkendorff, *Angew. Chem., Int. Ed.*, 2012, **51**, 4641–4643.
23 M. Peuckert, T. Yoneda, R. A. Dalla Betta and M. Boudart, *J. Electrochem. Soc.*, 1986, **133**, 944–947.
24 N. Giordano, E. Passalacqua, L. Pino, A. S. Arico, V. Antonucci, M. Vivaldi and K. Kinoshita, *Electrochim. Acta*, 1991, **36**, 1979–1984.
25 P. Brault, A. Caillard and A.-L. Thomann, *Chem. Vap. Deposition*, 2011, **17**, 296–304.
26 H. Qayyum, C.-J. Tseng, T.-W. Huang and S.-y. Chen, *Catalysts*, 2016, **6**, 180.
27 N. Todoroki, T. Kato, T. Hayashi, S. Takahashi and T. Wadayama, *ACS Catal.*, 2015, **5**, 2209–2212.
28 Y. Agawa, H. Tanaka, S. Torisu, S. Endo, A. Tsujimoto, N. Gonohe, V. Malgras, A. Aldalbahi, S. M. Alshehri, Y. Kamachi, C. Li and Y. Yamauchi, *Sci. Technol. Adv. Mater.*, 2015, **16**, 024804.
29 R. E. Palmer, R. Cai and J. Vernieres, *Acc. Chem. Res.*, 2018, **51**, 2296–2304.
30 J. Laskin, G. E. Johnson, J. Warneke and V. Prabhakaran, *Angew. Chem., Int. Ed.*, 2018, **57**, 16270–16284.
31 H. Tsunoyama, C. Zhang, H. Akatsuka, H. Sekiya, T. Nagase and A. Nakajima, *Chem. Lett.*, 2013, **42**, 857–859.
32 H. Tsunoyama, M. Shibuta, M. Nakaya, T. Eguchi and A. Nakajima, *Acc. Chem. Res.*, 2018, **51**, 1735–1745.
33 K. J. J. Mayrhofer, D. Strmcnik, B. B. Blizanac, V. Stamenkovic, M. Arenz and N. M. Markovic, *Electrochim. Acta*, 2008, **53**, 3181–3188.
34 T. Nagai, H. Murata and Y. Morimoto, *ECS Trans.*, 2012, **50**, 1539–1545.
35 B. Ravel and M. Newville, *J. Synchrotron Radiat.*, 2005, **12**, 537–541.
36 S. I. Zabinsky, J. J. Rehr, A. Ankudinov, R. C. Albers and M. J. Eller, *Phys. Rev. B: Condens. Matter Mater. Phys.*, 1995, **52**, 2995–3009.
37 G. Kresse and J. Hafner, *Phys. Rev. B: Condens. Matter Mater. Phys.*, 1993, **47**, 558–561.
38 G. Kresse and J. Hafner, *Phys. Rev. B: Condens. Matter Mater. Phys.*, 1994, **49**, 14251–14269.
39 Z. Zhao, E. F. Wang, H. Yan, Y. Kono, B. Wen, L. Bai, F. Shi, J. Zhang, C. Kenney-Benson, C. Park, Y. Wang and G. Shen, *Nat. Commun.*, 2015, **6**, 6212.
40 H. A. Hansen, V. Viswanathan and J. K. Nørskov, *J. Phys. Chem. C*, 2014, **118**, 6706–6718.
41 J. Zhang, M. B. Vukmirovic, Y. Xu, M. Mavrikakis and R. R. Adzic, *Angew. Chem.*, 2005, **117**, 2170–2173.
42 K. Bobuatong, S. Karanjit, R. Fukuda, M. Ehara and H. Sakurai, *Phys. Chem. Chem. Phys.*, 2012, **14**, 3103–3111.
43 L. G. Verga, J. Aarons, M. Sarwar, D. Thompsett, A. E. Russell and C.-K. Skylaris, *Phys. Chem. Chem. Phys.*, 2016, **18**, 32713–32722.
44 T. R. Garrick, T. E. Moylan, M. K. Carpenter and A. Kongkanand, *J. Electrochem. Soc.*, 2017, **164**, F55–F59.

